ANL/CMT/CP-96818

Spinel Electrodes for Lithium Batteries

by

Michael M. Thackeray
Argonne National Laboratory
Chemical Technology Division
Electrochemical Technology Program
9700 South Cass Avenue, B-205
Argonne, Illinois 60439 USA

November 1999

To be published in the Journal of the American Ceramic Society

DISCLAIMER

DISCLAIMER

Portions of this document may be illegible in electronic image products. Images are produced from the best available original document.

SPINEL ELECTRODES FOR LITHIUM BATTERIES

Michael M. Thackeray

Chemical Technology Division
Electrochemical Technology Program
Argonne National Laboratory
Argonne, Illinois 60439, USA

This paper gives a historical account of the development of spinel electrodes for rechargeable lithium batteries. Research in the late 1970's and early 1980's on high-temperature Li/Fe_3O_4 cells led to the evaluation of lithium spinels $Li[B_2]X_4$ at room temperature (B = metal cation). This work highlighted the importance of the $[B_2]X_4$ spinel framework as a host electrode structure and the ability to tailor the cell voltage by selection of different B cations. Examples of lithium-ion cells that operate with spinel anode/spinel cathode couples are provided. Particular attention is paid to spinels within the solid solution system $Li_{1+x}Mn_{2-x}O_4$ ($0 \leq x \leq 0.33$).

Introduction

The family of spinels is a very large one and contains many stable and robust materials. The prototype "spinel" is the mineral $MgAl_2O_4$, which exists in nature as a semi-precious gem [1]. Spinels have the general formula $A[B_2]X_4$, where A refers to the cations on tetrahedral (8a) sites, and B to the cations on octahedral (16d) sites of a cubic structure with space group symmetry Fd3m. The X anions, located at the 32e sites, form a cubic-close-packed array. There are 64 tetrahedral sites in a typical unit cell, one-eighth of which are occupied by the A cations, and 32 octahedral sites, one-half of which are occupied by the B cations. It would, therefore, appear at first glance that the unit cell of a spinel structure with 56 empty tetrahedral sites and

16 empty octahedral sites in the interstitial space would easily accommodate small guest ions such as lithium ions within its interstitial space. However, every empty tetrahedron and octahedron in the unit cell share at least two faces with the A tetrahedra or B octahedra. Therefore, the short distances and coulombic interactions between a guest ion on an interstitial site and the ions on an A or a B site prevent the simultaneous occupation of the interstitial sites and the A or B sites. It was, therefore, surprising when it was found that lithium ions could be introduced chemically and electrochemically into an $A[B_2]O_4$ spinel structure at room temperature with a concomitant reduction of the A- and B-type cations [2]. The reaction was understood when it was established that lithium insertion was accompanied by an internal phase change that transformed the spinel arrangement of cations to the cation arrangement of a rock-salt structure $[LiA]_{16c}[B_2]_{16d}O_4$, where the square brackets refer to crystallographically independent octahedral sites. Since the discovery that the lithium spinels $Li[B_2]O_4$ provide a stable three-dimensional interstitial space for the unrestricted movement of lithium ions through the spinel structure [3], researchers have shown great interest in exploiting this class of compounds as insertion electrodes for rechargeable lithium batteries. This interest has stemmed largely from the enormous growth in the electronics industry which is becoming increasingly dependent on lightweight, rechargeable batteries with high energy density. The production of rechargeable lithium-ion cells that started in 1990 grew to 100 million cells per year in 1996 and to 200 million cells in 1997 and is expected to increase to 600 million cells per year by the turn of the century. A longer-term application for lithium-ion batteries is electric-vehicle propulsion.

State-of-the-art lithium-ion batteries use a lithiated carbon negative electrode and a lithium cobalt oxide positive electrode. Because of the high cost of cobalt and concerns about its structural stability when cells are fully charged, increasing interest has been placed on the

lithium-manganese-oxide spinel $LiMn_2O_4$ as an alternative positive electrode for lithium-ion cells.

This review records the development of spinel technology for lithium batteries. A short section on high-temperature battery research that was conducted in the late 1970's and early 1980's is provided at the start of the review. This period of research highlighted the importance of the spinel structure as a component of the sodium-ion-conducting electrolyte, beta-alumina, in sodium batteries, and in iron oxide electrodes of lithium batteries; this period was largely responsible for many of the thought processes that led to the investigation of spinel electrodes for room-temperature lithium batteries. The account given in this review is a personal one; it is not intended to distract the reader from the vast and excellent research that has been conducted on spinel electrodes by many laboratories throughout the world over the last two decades. It is for brevity that only a limited number of references have been selected for this review.

High-Temperature Batteries

a) .Sodium/Sulfur and Sodium/Metal Chloride Batteries

The oil crisis of the 1970's spearheaded major international efforts to find alternative power sources to fossil fuels for transportation and energy storage. The discovery of a ceramic, beta-alumina, that exhibits a high sodium ion conductivity at 300°C [4] initiated major programs to develop high temperature sodium batteries, such as the 2-V Na/beta-alumina/S battery [5] and the 2.5-V Na/beta-alumina/$NaAlCl_4$, $NiCl_2$ ("Zebra") battery [6-8]. There are two structural forms of beta-alumina, designated β- and β''-alumina, corresponding to $Na_2O \bullet 11Al_2O_3$ and $Na_2O \bullet 5Al_2O_3$, respectively (Fig. 1) [9]. The structures are comprised of spinel blocks, each block containing four layers of close-packed oxygen ions with aluminum ions and stabilizing

lithium or magnesium ions occupying the tetrahedral and octahedral sites, as in the mineral "spinel". The sodium ions are located between the spinel blocks in oxygen-deficient layers; they are highly mobile because of the defects (vacancies) within the layers. The structures of β- and β''-alumina differ in the stacking arrangement of the spinel blocks at the conduction planes.

Safety concerns about Na/S batteries arose because of the violent reaction that can occur if molten sodium and molten sulfur combine at 300°C in failed cells. The safety hazards of Na/S batteries finally led to the termination of their development. The safety problem has been largely overcome in the related "Zebra" battery, in which the molten sulfur electrode is replaced with a solid $NiCl_2$ electrode and a molten salt electrolyte $NaAlCl_4$ (melting point = 154°C) [6-8].

b) Lithium/Iron Disulfide Battery

In 1973, a program at Argonne National Laboratory was initiated to develop a 1.8-V lithium battery with cells having the configuration LiAl/LiCl, KCl/FeS_2 [10-11]. The operating temperature of the battery is approximately 450°C. At this temperature, both metallic lithium and sulfur are molten. However, in the LiAl/LiCl, KCl/FeS_2 system, both lithium and sulfur electrodes are immobilized by using solid lithium-aluminum alloy and FeS_2 electrodes. Nevertheless, the system still requires expensive current collectors, such as molybdenum, to combat the highly corrosive sulfide electrode at high temperature. In an attempt to overcome these corrosion problems, iron oxide electrodes such as α-Fe_2O_3 (corundum-type structure) and Fe_3O_4 and $LiFe_5O_8$ (spinel structures) were investigated as alternative materials to FeS_2 in the early 1980's [12-16].

c) Lithium/Iron Oxide Cells

Lithium/iron oxide cells provide a relatively low voltage compared to lithium/iron sulfide cells; they deliver most of their capacity at approximately 1.1 V vs. LiAl, as shown in the

discharge profile of a LiAl/LiCl,KCl/Fe_3O_4 (spinel) cell at 400°C (Fig. 2) [13]. The voltage profile shows several discrete plateaus, each of which is associated with a three-phase reaction process. The nature of the electrochemical reaction can be understood from the Li-Fe-O phase diagram in Fig. 3. The reaction at the Fe_3O_4 electrode follows the dotted line toward the Li apex of the Li-Fe-O triangle until the Li_2O-Fe tie-line is reached; consequently, the composition of the electrode changes during discharge of the cell. During discharge, lithium ions are inserted into the tetrahedral and octahedral sites of the cubic-close-packed oxygen array with a concomitant extrusion of metallic iron. The Li:Fe ratio in the oxide thus increases during discharge, thus resulting in the successive formation of $LiFe_5O_8$, $LiFeO_2$, Li_5FeO_4, and finally Li_2O at the electrode. The overall reaction sequence for the electrochemical reaction at a Fe_3O_4 electrode is shown below, where the round brackets refer to ions in tetrahedral sites and the square brackets refer to ions in octahedral sites. Of significance, is that the oxygen array remains fixed and essentially unaltered during the whole reaction. Site positions are given in accordance with the cubic space group Fd3m.

$(Fe)_{8a}[Fe_2]_{16d}O_4$	Fe_3O_4	spinel
↕ 0.5 Li	↕ Li	↕
$(Fe)_{8a}[Fe_{1.5}Li_{0.5}]_{16d}O_4$ + 0.5 Fe	$LiFe_5O_8$	spinel
↕ 1.5 Li	↕ Li	↕
$[FeLi]_{16c}[FeLi]_{16d}O_4$ + Fe	$LiFeO_2$	rock salt
↕ 6 Li (via Li_5FeO_4)	↕ Li	↕
$(Li_8)_{8a,8b\ 48f}O_4$ + 3 Fe	Li_2O	anti-fluorite

If α-Fe_2O_3 is used as the cathode material, lithium insertion causes the hexagonally-close-packed array of the corundum-type structure to shear irreversibly to cubic-close-packing to generate a defect spinel structure. Thereafter, the reaction sequence follows the dotted line between Fe_2O_3 and Li in Fig. 3, and is similar to the reaction described above [15]. Because the final discharge product (Li_2O) is slightly soluble in the molten salt electrolyte at 400°C, lithium/iron oxide cells lose capacity slowly on cycling if deeply discharged. Nevertheless, the reaction is reversible, and hundreds of cycles are achievable if cells are only partially discharged [14].

Room-Temperature Lithium/Iron Oxide Cells

The realization that iron oxides with a close-packed oxygen array are electrochemically active toward lithium at 400°C, and that spinel-type structures are the stable phases at the top of charge led to an electrochemical study of magnetite in room temperature cells. The voltage profile of a Li/1M $LiClO_4$ in propylene carbonate/Fe_3O_4 cell is shown in Fig. 4 [2]. This voltage profile clearly differs from that of high temperature Li/Fe_3O_4 cells. The data show that lithium can be inserted into the Fe_3O_4 spinel structure in a single-phase process to an approximate composition $LiFe_3O_4$. These data and X-ray diffraction analyses of lithiated $Li_xFe_3O_4$ electrodes revealed that the tetrahedral site ions were displaced during the initial stage of the electrochemical reaction into neighboring octahedral sites. Thereafter, the voltage profile is indicative of a two-phase process, which can be attributed to the displacement of metallic iron from the oxide structure. The generalized reaction at the electrode can thus be represented as a two-stage process:

$$(Fe)_{8a}[Fe_2]_{16d}O_4 \xrightarrow{1)\ Li} [LiFe]_{16c}[Fe_2]_{16d}O_4 \xrightarrow[(x_{max}=3)]{2)\ x\ Li} Li_{1+2.33x}Fe_{3-x}O_4 + x\ Fe$$

On the initial insertion of lithium, the tetrahedral-site iron ions are cooperatively displaced into octahedral (16c) sites to generate a defect rock-salt structure $[Li_\delta\square_{1-\delta}Fe]_{16c}[Fe_2]_{16d}O_4$, where $\square$ refers to a vacancy. Lithiation continues until the rock-salt stoichiometry $[LiFe]_{16c}[Fe_2]_{16d}O_4$ is reached. During this process, the $[Fe_2]_{16d}O_4$ spinel framework remains intact. This reaction is irreversible below 3 V because of the kinetic barrier that prevents lithium extraction from a rock-salt type structure that has 75% of the octahedral sites fully occupied with iron and, thus, has no unrestricted pathways for lithium-ion diffusion. During the second stage of the reaction, metallic iron is extruded from the rock-salt structure to accommodate the incoming lithium ions.

Lithium Spinel Electrodes $Li[B_2]X_4$

The discovery that lithium spinels $Li[B_2]X_4$ (B = metal cation) could accommodate lithium and that the $[B_2]X_4$ provided a host framework with a three-dimensional interstitial space for lithium insertion and extraction heralded the start of an intense search for stable spinel electrodes for rechargeable lithium batteries. Moreover, the ability to place a wide variety of transition metal cations on the B sites of the spinel framework makes it possible to tailor the voltage of a lithium cell. Table 1 lists the operating voltages of several $Li/Li[B_2]X_4$ spinel couples. In principle, therefore, it is possible to couple spinel anodes with spinel cathodes to provide lithium-ion cells with a range of working voltages [17].. For example, a $Li_{4+x}Ti_5O_{12}/Li_{1-x}Mn_2O_4$ couple would provide a 2.5 V cell, and a $Li_{4+x}Ti_5O_{12}/ Li_{7-x}Mn_5O_{12}$ couple

would provide a 1.5 V cell. A schematic illustration of such a spinel anode/spinel cathode lithium-ion cell is shown in Fig. 5.

(INSERT TABLE 1 HERE TO KEEP CORRECT SEQUENCE OF REFERENCES)

Spinel $Li_4Ti_5O_{12}$

The spinel $Li_4Ti_5O_{12}$ has structural properties that make it an ideal insertion electrode for lithium battery applications. It has the spinel notation $Li[Ti_{1.67}Li_{0.33}]O_4$. Lithium is inserted into the spinel structure according to the reaction

$$Li + (Li)_{8a}[Ti_{1.67}Li_{0.33}]_{16d}O_4 \text{ ------ > } [Li_2]_{16c}[Ti_{1.67}Li_{0.33}]_{16d}O_4$$

As with all $Li[B_2]X_4$ spinels, lithium insertion causes a cooperative displacement of the tetrahedral-site lithium ions into neighboring octahedral sites; the reaction generates the rock-salt phase $[Li_2]_{16c}[Ti_{1.67}Li_{0.33}]_{16d}O_4$. It is thus a two-phase reaction that provides a constant voltage response at 1.5 V vs. Li (Fig. 6a) [17, 19, 20]. The cubic symmetry of the parent spinel is unaffected by lithiation; the lattice parameter (8.36 Å) and unit cell volume are virtually unaltered by the phase transition. The lack of any significant change to the crystallographic parameters is remarkable and provides a structure that is extremely tolerant to electrochemical cycling (Fig. 6b) [19, 20, 32]. The excellent stability of a $Li/Li_4Ti_5O_{12}$ cell to electrochemical cycling is shown in Fig. 6a, in which the voltage profiles of the 10^{th}, 20^{th} and 30^{th} cycles are super-imposable and cannot be distinguished from one another [32]. Unfortunately, the low theoretical capacity of $Li_4Ti_5O_{12}$ (163 mAh/g) compared to other transition metal oxides, such as MnO_2 (308 mAh/g), and the relatively low oxidation potential (1.5 V vs. Li) limit the energy density of cells that use $Li_4Ti_5O_{12}$ electrodes. Despite these disadvantages, $Li_4Ti_5O_{12}$ is an extremely attractive negative electrode for relatively low-voltage lithium-ion cells because they eliminate the safety hazards of negative electrodes that operate close to the potential of metallic

lithium. For example, the good cycling stability of a 2.5-V cell containing a $Li_4Ti_5O_{12}$ negative electrode and a stabilized manganese spinel positive electrode of composition $LiZn_{0.025}Mn_{1.95}O_4$ is shown in Fig. 7; also provided are the voltage profiles of both electrodes, monitored against a metallic lithium reference electrode [17, 33].

The Li-Mn-O Spinel System

Many stoichiometric spinel compounds exist in the Li-Mn-O system. Their compositions reside on the tie-line between Mn_3O_4 (hausmannite) and $Li_4Mn_5O_{12}$ in the Li-Mn-O phase diagram (Fig. 8) [34]. The spinel compositions of interest for rechargeable lithium battery applications lie on the tie-line between $LiMn_2O_4$ and $Li_4Mn_5O_{12}$. These compounds can be represented by the general formula $Li_{1+x}Mn_{2-x}O_4$ [34-37].

a) *$Li[Mn_2]O_4$*

$Li[Mn_2]O_4$ is the most extensively studied spinel of the Li-Mn-O system. Lithium insertion into $Li[Mn_2]O_4$ takes place at 2.96 V (open-circuit voltage) according to the two-phase reaction [23]:

$$Li + Li[Mn_2]O_4 \text{ -----} > Li_2[Mn_2]O_4$$

in which the spinel phase $Li[Mn_2]O_4$ is transformed in a first-order reaction to the rock-salt phase $Li_2[Mn_2]O_4$. The increase in the concentration of Mn^{3+} (d^4, Jahn-Teller) ions reduces the cubic symmetry of the $Li[Mn_2]O_4$ spinel phase (a = 8.248 Å) to tetragonal symmetry in the $Li_2[Mn_2]O_4$ rock-salt phase (a = 8.007 Å, c = 9.274 Å) [23, 38]. The phase transition causes a 16% increase in the c/a ratio of the unit cell. Such a large anisotropic change in the lattice parameters is too severe for the host electrode to maintain its structural integrity on cycling. Thus, $Li/Li[Mn_2]O_4$ cells suffer a rapid capacity fade on cycling at 3 V(Fig. 9a). By contrast, electrochemical

extraction of lithium from the tetrahedral sites of $Li[Mn_2]O_4$ does not alter the cubic symmetry of the spinel electrode [29-31]. This reaction takes place at approximately 4 V vs. Li. As a result, $Li[Mn_2]O_4$ electrodes show superior cycling over the high voltage range (Fig. 9b). It is difficult to electrochemically extract all the lithium from $Li[Mn_2]O_4$. However, earlier work by Hunter demonstrated that essentially all the lithium could be removed from $Li[Mn_2]O_4$ by chemical reaction with acid according to the reaction [39]:

$$2\,Li[Mn_2]O_4 \text{ ----> } 3\,\lambda\text{-}MnO_2 + MnO + Li_2O$$

This chemical reaction removes the lithium (as Li_2O) from the spinel; 25% of the manganese is also lost from the structure by dissolution as MnO. Perhaps surprisingly, the product, λ-MnO_2, still crystallizes with the $[Mn_2]O_4$ spinel framework. The λ-MnO_2 structure is unstable to heat treatment and transforms to β-MnO_2 with a rutile-type structure at approximately 270°C [39]; its high reduction potential and high reactivity as a fully charged electrode, the necessity to dry the material before use, and its instability to heat-treatment make λ-MnO_2 an unattractive electrode compared to $Li[Mn_2]O_4$. The latter compound, which is prepared dry, has a stable and robust stoichiometric spinel structure, and is loaded in the discharged state in 4-V lithium-ion cells.

Much work has been done in recent years in an attempt to replace the costly positive electrode of commercial $Li_xC_6/Li_{1-x}CoO_2$ lithium-ion cells with a $Li[Mn_2]O_4$ spinel electrode. Despite the structural robustness of $Li[Mn_2]O_4$ and the advantage that $Li_{1-x}[Mn_2]O_4$ electrodes expand and contract isotropically over the compositional range $0<x<1$ at 4 V vs. Li, lithium-ion cells with $Li_{1-x}[Mn_2]O_4$ electrodes still show a slow capacity fade at room temperature, which is accentuated if the operating temperature of the cells is raised to 40 to 50°C, i.e., a temperature

that can be reached in devices such as laptop computers. The capacity fade of these cells has been attributed to three factors:

1. Solubility of the spinel electrode, for example, by acid attack from the electrolyte, and by a disproportionation reaction at the particle surface [34, 40-44].

$$2\,Mn^{3+}_{(solid)} \text{ -----> } Mn^{4+}_{(solid)} + Mn^{2+}_{(solution)}$$

2. An instability of a highly delithiated spinel $Li_{1-x}[Mn_2]O_4$, resulting, for example, from oxygen loss at the particle surface as the cell approaches the top of charge [34]. The loss of oxygen and concomitant reduction of Mn^{4+} to Mn^{3+} ions at 4 V is most likely related to oxidation of the electrolyte and dissolution of the spinel according to the disproportionation reaction given above.

3. The onset of a damaging Jahn-Teller distortion at the particle surface of the spinel electrode at the end of discharge (above 3 V) under dynamic, non-equilibrium conditions [34]. Recent electron diffraction and imaging data obtained from cycled $Li_{1-x}[Mn_2]O_4$ electrodes have provided evidence that, under high rate conditions, the tetragonal $Li_2[Mn_2]O_4$ phase is formed at the surface of some spinel particles above the expected thermodynamic voltage (2.96 V), thus causing structural damage to the electrode (Figs. 10, 11) [45].

Improved capacity retention can be achieved by substituting some of the manganese ions in the $[B_2]X_4$ spinel framework with a mono- , di- or trivalent cation. This substitution raises the average oxidation state of the stoichiometric spinel compound marginally above 3.5 [34]. For example, the average manganese oxidation state of the spinel $Li_{1.05}Mn_{1.95}O_4$, which lies close to $Li[Mn_2]O_4$ on the $Li[Mn_2]O_4$-$Li_4Mn_5O_{12}$ tie-line in Fig. 8, is 3.56. This spinel composition has several advantages. First, lithium extraction can only take place to $Li_{0.2}Mn_{1.95}O_4$, at which

composition the manganese ions are fully oxidized; the 0.2 Li that remain in the structure (0.15 of which are located in the interstitial channels of a $[Mn_{1.95}Li_{0.05}]O_4$ framework) stabilize the electrode structure at the top of charge. Second, the increase in Mn^{4+} content in the stoichiometric spinel may suppress the disproportionation reaction shown above. Third, at the end of discharge, for example at 3.3 V, when the electrode approaches the stoichiometric spinel composition $Li_{1.05}Mn_{1.95}O_4$, the average oxidation state of the manganese ions is above the expected value for the onset of the Jahn-Teller distortion, thereby stabilizing the surface of the electrode to overlithiation. The radical improvement in capacity retention in a room temperature cell with a lithium-rich spinel electrode of composition $Li_{1.03}Mn_{1.97}O_4$ compared to a cell with a standard $Li[Mn_2]O_4$ electrode is shown in Fig. 12 [34].

b) *$Li_4Mn_5O_{12}$*

$Li_4Mn_5O_{12}$ is an end member of the $Li_{1+x}Mn_{2-x}O_4$ system (x = 0.33); it has the spinel notation $Li[Mn_{1.67}Li_{0.33}]O_4$. Unlike $Li[Mn_2]O_4$, which can act as a 3-V electrode (when lithium is inserted into the interstitial octahedral sites of the structure) or a 4-V electrode (when lithium is extracted from the tetrahedral sites), $Li_4Mn_5O_{12}$ operates only as a 3-V electrode because all the manganese ions are tetravalent, and therefore, lithium cannot be extracted from the structure. The $Li_{4+x}Mn_5O_{12}$ electrode remains cubic over a wide compositional range at 3 V, the Jahn-Teller distortion occurring only late in the discharge at the composition $Li_{6.5}Mn_5O_{12}$ (x = 2.5), when the manganese oxidation state reaches 3.5 [26]. Moreover, the extent of the Jahn-Teller effect in the fully lithiated rock-salt phase $Li_7Mn_5O_{12}$ (x=3, c/a = 1.106) is not as severe as it is in $Li_2Mn_2O_4$ (c/a = 1.163) [23, 38]. These data highlight the flexibility of the Li-Mn-O spinel system and demonstrate that it is possible to select different spinel compositions that allow the cubic symmetry of the electrode to be maintained at either 3 V or 4 V, thus providing systems with

good cycle life at two distinct voltages. Excellent cycling performance at 3 V has recently been reported for $Li_4Mn_5O_{12}$ [27].

Composite Lithium-Manganese-Oxide Electrodes

The tendency for several lithium-manganese-oxide materials to transform to a spinel structure, usually within the solid solution system $Li_{1+x}Mn_{2-x}O_4$, either on heating or during the insertion and extraction of lithium in an electrochemical cell, highlights the stability and robustness of spinel compounds. For example, lithiated MnO_2 structures with the composition $Li_{0.5}MnO_2$, whether derived from ramsdellite-MnO_2 or α-MnO_2, or from delithiated $LiMnO_2$ structures, transform readily to $Li[Mn_2]O_4$ on heating at 300°C under an inert atmosphere [46]. γ-MnO_2 electrodes that are heated with LiOH in a 7:3 molar ratio at 350-420°C in air consist of a composite structure that is composed of domains of a lithiated-γ-MnO_2 phase and domains of a spinel phase [47-51]; the composite electrode has been given the acronym "CDMO" (Composite Dimensional Manganese Oxide) by Sanyo [47, 48]. Orthorhombic-$LiMnO_2$ and layered-$LiMnO_2$ structures transform to a spinel structure on electrochemical cycling of lithium [52-58]; the resulting products are not single phase, but are also composite structures containing domains of spinel and domains of the residual parent structure [58].

The inherent stability of the spinel structure plays an important role in stabilizing these composite electrodes. For example, γ-MnO_2 and ramsdellite-MnO_2 structures have a distorted hexagonally close-packed oxygen array that is unstable to lithiation; the close-packed oxygen array shears on lithiation toward a more stable cubic-close-packed structure [46, 59]; the same effect occurs when γ-MnO_2 reacts with LiOH to generate "CDMO" type products [49]. The enhanced stability of "CDMO" electrodes in lithium cells compared to pure γ-MnO_2 electrodes

has been attributed to the presence of the spinel domains in the structure and to the compatibility of the close-packed oxygen arrays of the spinel- and lithiated-γ-MnO_2 phases. Both structure types have been identified in "CDMO" products by electron diffraction data and high- resolution imaging of crystallites in the electrode (Fig. 13) [51]. In electrochemically delithiated orthorhombic-$LiMnO_2$ and layered-$LiMnO_2$ structures, spinel domains have been found to be intergrown with domains derived from the parent $LiMnO_2$ structures (Fig. 14) [58]. Composite structures derived from these $LiMnO_2$ materials show voltage profiles typical of spinel electrodes, and can be cycled over the 4 V and 3 V regions with far better capacity retention than standard $Li[Mn_2]O_4$ spinel electrodes. This good cycling behavior has been attributed, in particular, to spinel domains with compositions within the $Li_{1+x}Mn_{2-x}O_4$ system ($0<x\leq0.33$) that are more tolerant to cycling over the lower voltage regime than $Li[Mn_2]O_4$.

Conclusions

The family of lithium spinels $Li[B_2]O_4$ (B = metal cation) provides a wide range of materials that are of interest as insertion electrodes for lithium batteries. Much of the recent research has been spent on developing lithium-manganese-oxide spinel electrodes for 3- and 4-V battery applications. The role that spinel domains play in stabilizing electrode structures has been stressed. These domains, in general, are derived from the stoichiometric (3 V) spinels along the $Li[Mn_2]O_4$-$Li_4Mn_5O_{12}$ tie-line in the Li-Mn-O phase diagram. They stabilize not only the surface of "4 V" $Li_{1-x}[Mn_2]O_4$ electrodes at the end of discharge, but also composite electrode structures derived, for example, from γ-MnO_2, layered-$LiMnO_2$ and orthorhombic-$LiMnO_2$. The lithium-titanate spinel $Li_4Ti_5O_{12}$ is particularly attractive as a negative electrode for low-voltage

lithium-ion cells and for reducing the safety hazards associated with conventional high-voltage (4 V) lithium-ion batteries.

Acknowledgments

Y. Shao-Horn and S. A. Hackney of Michigan Technological University are thanked for their unpublished electron diffraction patterns of the "CDMO" products. Support from the U.S. Department of Energy's Advanced Battery Program, Chemical Science Division, Office of Basic Energy Sciences, under contract No. W-31-109-Eng-38 is gratefully acknowledged.

References

1. R. W. Hughes, *Ruby and Sapphire*, RWH Publishing, Boulder, Colorado (1997).
2. M. M. Thackeray, W. I. F. David and J. B. Goodenough, *Mat. Res. Bull.*, **17**, 785-793 (1982).
3. M. M. Thackeray and J. B. Goodenough, U.S. Patent 4,507,371 (1985).
4. R. W. Glazebrook, in *Power Sources for Electric Vehicles* (Eds. B. D. McNicol and D. A. J. Rand), Elsevier, Amsterdam, p. 657-692 (1984).
5. J. Sudworth and R. Tilley, *The Sodium/Sulfur Battery*, Chapman and Hall, London (1985).
6. J. Coetzer, *J. Power Sources*, **18**, 377-380 (1986).
7. R. C. Galloway, *J. Electrochem. Soc.*, **134**, 256-257 (1987).
8. J. Sudworth, *J. Power Sources*, **51**, 105-114 (1994).
9. G. K. Duncan, M. M. Thackeray and A. Van Zyl, *Archimedes*, **29**, 10-12 (1987).

10. D. R. Vissers, Z. Tomczuk and R. K. Steunenberg, *J. Electrochem. Soc.*, **121,** 665-667 (1974).

11. T. D. Kaun, P. A. Nelson, L. Redey, D. R. Vissers and G. L. Henriksen, *Electrochimica Acta*, **38**, 1269-1287 (1993).

12. N. A. Godshall, I. D. Raistrick and R. A. Huggins, *Mat. Res. Bull.*, **15**, 561-568 (1980).

13. N. A. Godshall, I. D. Raistrick and R. A. Huggins, *J. Electrochem. Soc.*, **131,** 543-549 (1984).

14. M. M. Thackeray and J. Coetzer, *Mat. Res. Bull.*, **16**, 591-597 (1981).

15. M. M. Thackeray, W. I. F. David and J. B. Goodenough, *J. Solid State Chem.*, **55**, 280-286 (1984).

16. L. A. de Picciotto and M. M. Thackeray, *Mat. Res. Bull.*, **21**, 583-592 (1986).

17. E. Ferg, R. J. Gummow, A. de Kock and M. M. Thackeray, *J. Electrochem. Soc.*, **141**, L147-L150 (1994).

18. D. W. Murphy, R. J. Cava, S. M. Zahurak and A. Santoro, *Solid State Ionics*, **9-10**, 413-418 (1983).

19. K. M. Colbow, J. R. Dahn and R. R. Haering, *J. Power Sources*, **26**, 397-402 (1989).

20. T. Ohzuku, A. Ueda and N. Yamamoto, *J. Electrochem. Soc.*, **142**, 1431-1435 (1995).

21. L. A. de Picciotto and M. M. Thackeray, *Solid State Ionics*, **18&19**, 773-777 (1985).

22. L. Guohua, S. Sakuma, H. Ikuta, T. Uchida, M. Wakihara and G. Hetong, *Denki Kagaku*, **64**, 202-206 (1996).

23. M. M. Thackeray, W. I. F. David, P. G. Bruce and J. B. Goodenough, *Mat. Res. Bull.*, **18**, 461-472 (1983).

24. J. B. Goodenough, M. M. Thackeray, W. I. F. David and P. G. Bruce, *Rev. de Chim. Min.*, **23**, 435-455 (1984).

25. A. de Kock, M. H. Rossouw, L. A. de Picciotto, M. M. Thackeray, W. I. F. David and R. M. Ibberson, *Mat. Res. Bull.*, **25**, 657-664 (1990).

26. M. M. Thackeray, A. de Kock, M. H. Rossouw, D. C. Liles, R. Bittihn and D. Hoge, *J. Electrochem. Soc.*, **139**, 363-366 (1992).

27. J. Kim and A. Manthiram, *J. Electrochem. Soc.*, **145**, L53-L55 (1998).

28. Y. Shao-Horn, S. A. Hackney, C. S. Johnson, A. J. Kahaian and M. M. Thackeray, *J. Solid State Chem.*, (1998). In press.

29. M. M. Thackeray, P. J. Johnson, L. A. de Picciotto, P. G. Bruce and J. B. Goodenough, *Mat. Res. Bull.*, **19**, 179-187 (1984).

30. T. Ohzuku, M. Kitagawa and T. Hirai, *J. Electrochem. Soc.*, **137**, 769-775 (1990).

31. J. M. Tarascon, E. Wang, F. K. Shokoohi, W. R. McKinnon and S. Colson, *J. Electrochem. Soc.*, **138**, 2859-2864 (1991).

32. A. N. Jansen, A. J. Kahaian, K. D. Kepler, K. Amine, D. W. Dees, D. R. Vissers and M. M. Thackeray, *J. Power Sources* (1998). Submitted.

33. M. M. Thackeray, *J. Electrochem. Soc.*, **142**, 2558-2563 (1995).

34. R. J Gummow, A. de Kock and M. M. Thackeray, *Solid State Ionics*, **69**, 59-67 (1994).

35. C. Masquelier, M. Tabuchi, K. Ado, R. Kanno, Y.Kobayashi, Y. Maki, O. Nakamura and J. B. Goodenough, *J. Solid State Chem.*, **123**, 255-266 (1996).

36. P. Strobel, F. Le Cras and M. Anne, *J. Solid State Chem.*, **124**, 83-94 (1996).

37. Y. Gao, J. N. Reimers and J. R. Dahn, *Phys. Rev. B*, **54**, 3878-3883 (1996).

38. A. Mosbah, A. Verbaere and M. Tournoux, *Mat. Res. Bull.*, **18**, 1375-1381 (1983).

39. J. C. Hunter, *J. Solid State Chem.*, **39**, 142-147 (1981).

40. D. H. Jang, Y. J. Shin and S. M. Oh, *J. Electrochem. Soc.*, **143**, 2204-2211 (1996).

41. G. G. Amatucci, C. N. Schmutz, A. Blyr, C. Sigala, A. S. Gozdz, D. Larcher and J. M. Tarascon, *J. Power Sources*, **69**, 11-25 (1997).

42. Y. Xia, Y. Zhou and M. Yoshio, *J. Electrochem. Soc.*, **144**, 2593-2600 (1997).

43. D. H. Jang and S. M. Oh, *J. Electrochem. Soc.*, **144**, 3342-3348 (1997).

44. A. Blyr, C. Sigala, G. G. Amatucci, D. Guyomard, Y. Chabres, and J. M. Tarascon, *J. Electrochem. Soc.* **145**, 194-209 (1998).

45. M. M. Thackeray, Y. Shao-Horn, A. J. Kahaian, K. D. Kepler, E. Skinner, J. T. Vaughey and S. A. Hackney, *Electrochemical and Solid State Letters.*, **1**, 7-9 (1998).

46. M. M. Thackeray, M. H. Rossouw, R. J. Gummow, D. C. Liles, K. Pearce, A. de Kock, W. I. F. David and S. Hull, *Electrochim. Acta*, **38**, 1259-1267 (1993).

47. T. Nohma, T. Saito, N. Furukawa and H. Ikeda, *J. Power Sources*, **26**, 389-396 (1989).

48. T. Nohma, Y. Yamamoto, I. Nakane and N. Furukawa, *J. Power Sources*, **39**, 51-57 (1992).

49. M. M. Thackeray, M. H. Rossouw, A. de Kock, A. P. de la Harpe, R. J. Gummow, K. Pearce and D. C. Liles, *J. Power Sources*, **43-44**, 289-300 (1993).

50. L. Li and G. Pistoia, *Solid State Ionics*, **47**, 241-249 (1991).

51. Y. Shao and S. Hackney, Ext. Abstr., 189th Meeting of the Electrochemical Society, Los Angeles (5-10 May), p. 58 (1996).

52. R. J. Gummow and M. M. Thackeray, *J. Electrochem. Soc.*, **141**, 1178-1182 (1994).

53. I. Koetschau, M. N. Richard, J. R. Dahn, J. B. Soupart and J. C. Rousche, *J. Electrochem. Soc.*, **142**, 2906-2910 (1995).

54. I. J. Davidson, R. S. McMillan, J. J. Murray and J. E. Greedan, *J. Power Sources*, **54**, 232-235 (1995).

55. A. R. Armstrong and P. G. Bruce, *Nature*, **381**, 499-500 (1996).

56. F. Capitaine, P. Gravereau and C. Delmas, *Solid State Ionics*, **89**, 197-202 (1996).

57. G. Vitins and K. West, *J. Electrochem. Soc.*, **144**, 2587-2592 (1997).

58. Y. Shao-Horn, S. A. Hackney, A. R. Armstrong, P. G. Bruce, R. Gitzendanner, C. S. Johnson and M. M. Thackeray, *J. Electrochem. Soc.*, (1997). In press.

59. T. Ohzuku, M. Kitagawa and T. Hirai, *J. Electrochem. Soc.*, **136**, 3169-3174 (1989).

Captions to Figures

Fig. 1. Schematic illustrations of the structures of β- and β''-alumina [9].

Fig. 2. The equilibrium potential profile of a $Li/Li_xFe_3O_4$ cell at 400°C [13].

Fig. 3. The Li-Fe-O phase diagram at 400°C [13].

Fig. 4. The equilibrium potential profile of a $Li/Li_xFe_3O_4$ cell at room temperature [14].

Fig. 5. A schematic illustration of a spinel anode/spinel cathode lithium-ion cell.

Fig. 6. Electrochemical properties of a $Li/Li_4Ti_5O_{12}$ cell [20].

Fig. 7. Electrochemical cycling behavior of a $Li_4Ti_5O_{12}/LiZn_{0.025}Mn_{1.95}O_4$ cell [20].

Fig. 8. Section from the Li-Mn-O phase diagram at room temperature [23].

Fig. 9. Cycling performance of (a) a 3-V $Li/Li_{1+x}Mn_2O_4$ cell, charged and discharged between 3-3 and 2.2 V and (b) a 4-V $Li/Li_{1-x}Mn_2O_4$ cell, charged and discharged between 4.2 and 3.0 V [45].

Fig. 10. Electron diffraction patterns ([100] zone axis) of (a) a cubic $LiMn_2O_4$ crystallite and (b) a tetragonal $Li_2Mn_2O_4$ lithiated spinel crystallite on the surface of an $LiMn_2O_4$ electrode particle (discharged from 4.2 to 3.3 V) [38].

Fig. 11. Transmission electron microscope image of an $Li_xMn_2O_4$ spinel electrode discharged in a lithium cell from 4.2 to 3.3 V. The black lines (arrowed) indicate the boundary between a tetragonal $Li_2Mn_2O_4$ crystallite and a cubic $LiMn_2O_4$ crystallite [38].

Fig. 12. Electrochemical profiles of 4 V $Li_{1+\delta}Mn_{2-\delta}O_4$ cells ($\delta = 0$ and $\delta = 0.03$) showing the improved capacity retention in the lithium-rich sample [23].

Fig. 13. Electron diffraction patterns of (a) a cubic spinel phase ([100] zone axis) and (b) a lithiated γ-MnO_2 phase with orthorhombic symmetry ([1-20] zone axis) in a "CDMO" electrode [45].

Fig. 14. Microstructure of a $Li_{0.5}MnO_2$ crystallite derived from layered $LiMnO_2$, showing an irregular lattice image associated with microdomains of spinel embedded within a residual Li_xMnO_2 structure.

Table 1: Electrochemical Li/Li$[B_2]X_4$ Spinel Couples

Cell Couple	x_{max}	Approximate Operating Voltage (V)
$Li/Li_{1+x}Ti_2O_4$ [18, 19]	1	1.4
$Li/Li_{4+x}Ti_5O_{12}$ [19, 20]	3	1.5
$Li/Li_{1+x}V_2O_4$ [21, 22]	1	2.3 to 1.3 (two stage)
$Li/Li_{1+x}Mn_2O_4$ [23, 24]	1	2.8
$Li/Li_{2+x}Mn_4O_9$ [25]	3	2.8
$Li/Li_{4+x}Mn_5O_{12}$ [26, 27]	3	2.8
$Li/Li_{2-x}Co_2O_4$ [28]	~1	3.4
$Li/Li_{1-x}Mn_2O_4$ [29-31]	~1	4.0

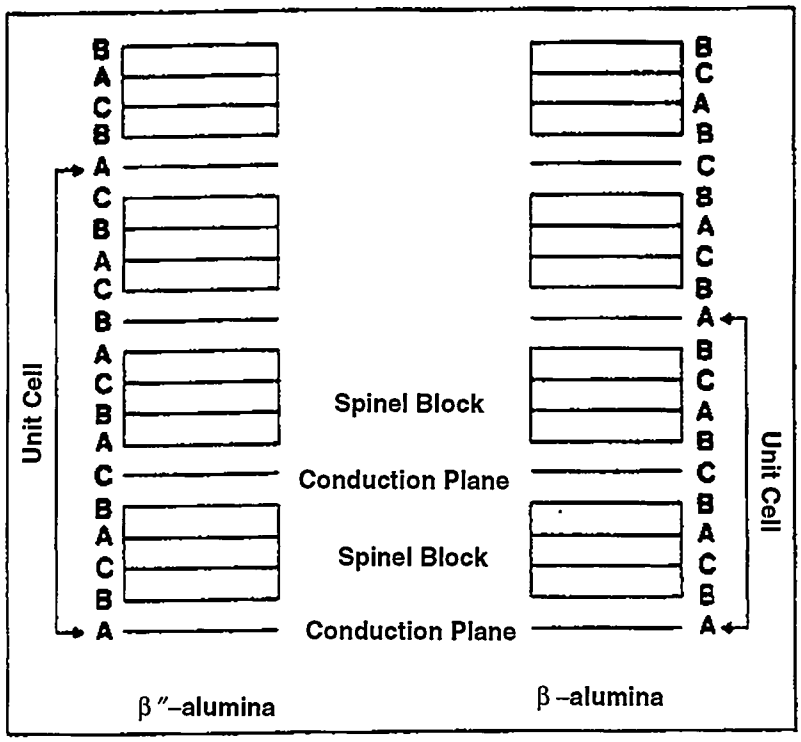

Figure 1

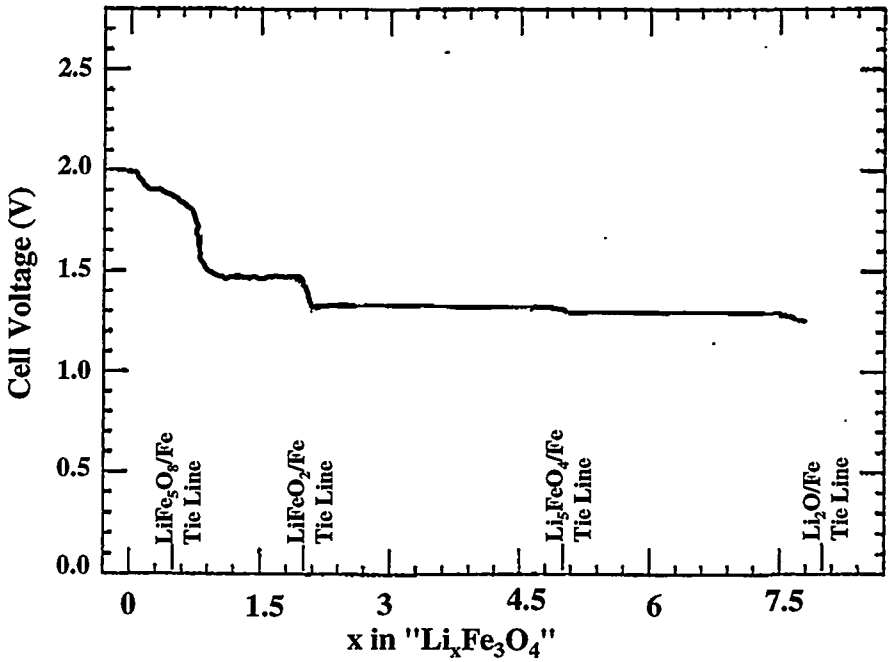

Figure 2

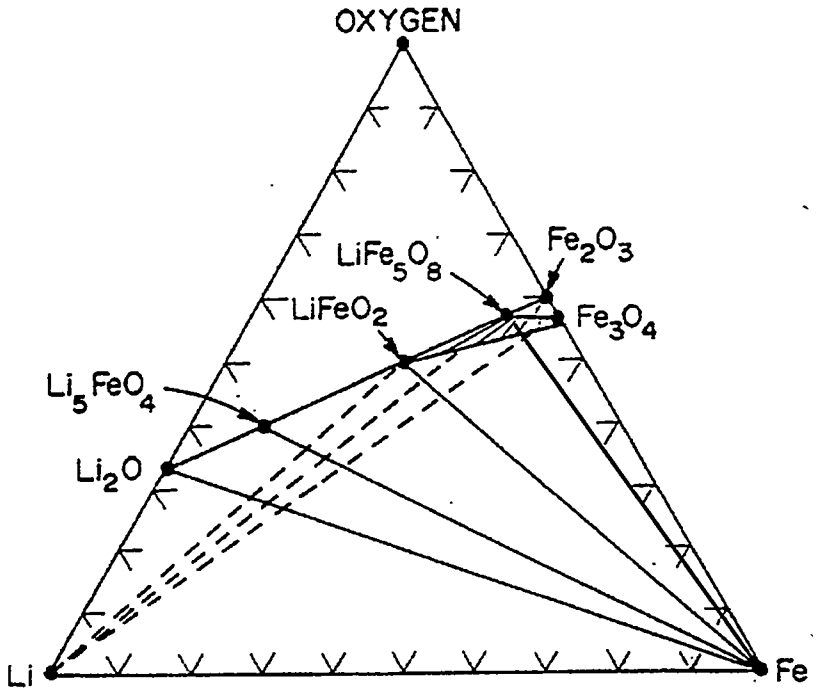

Figure 3

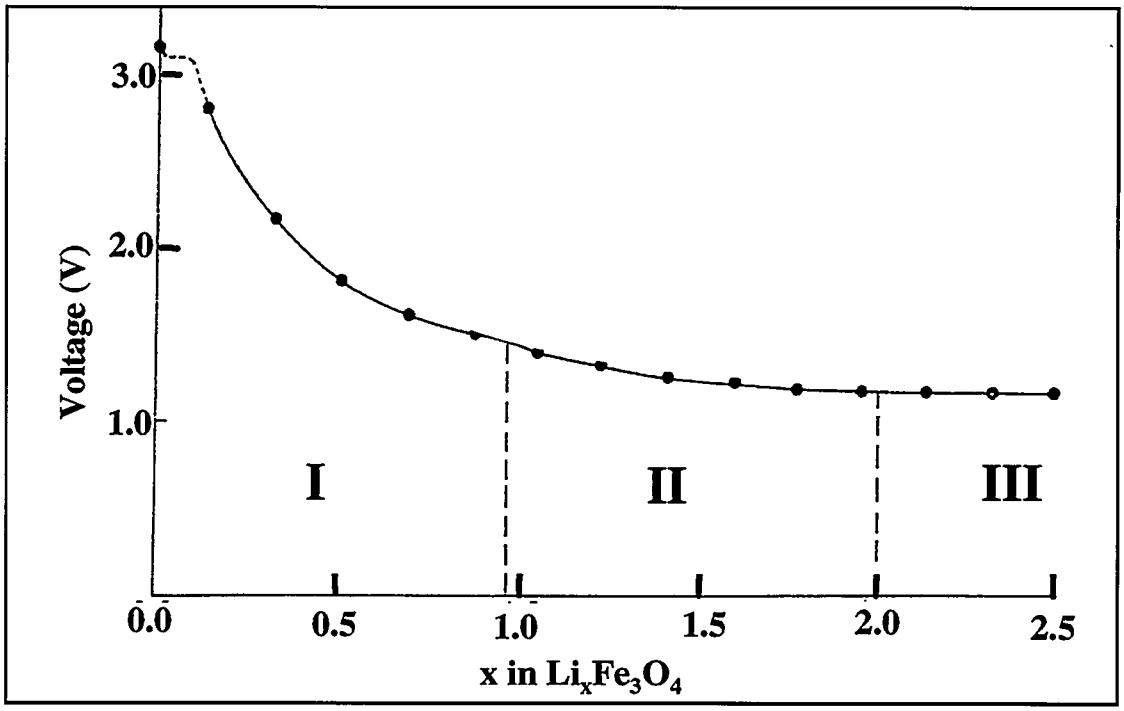

Figure 4

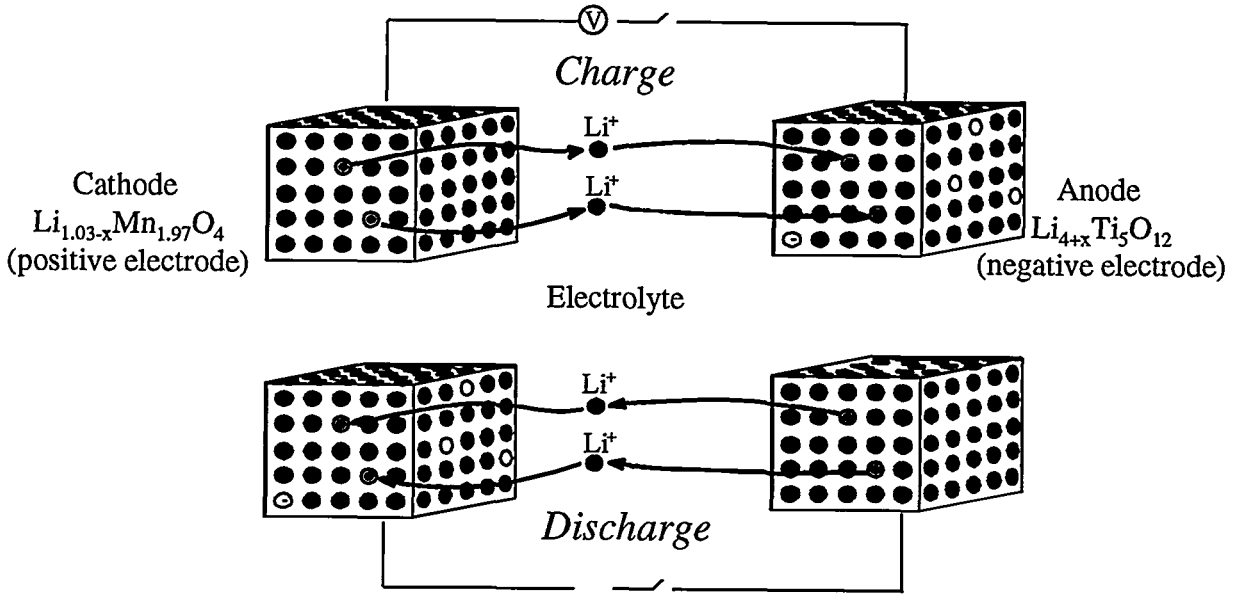

Figure 5

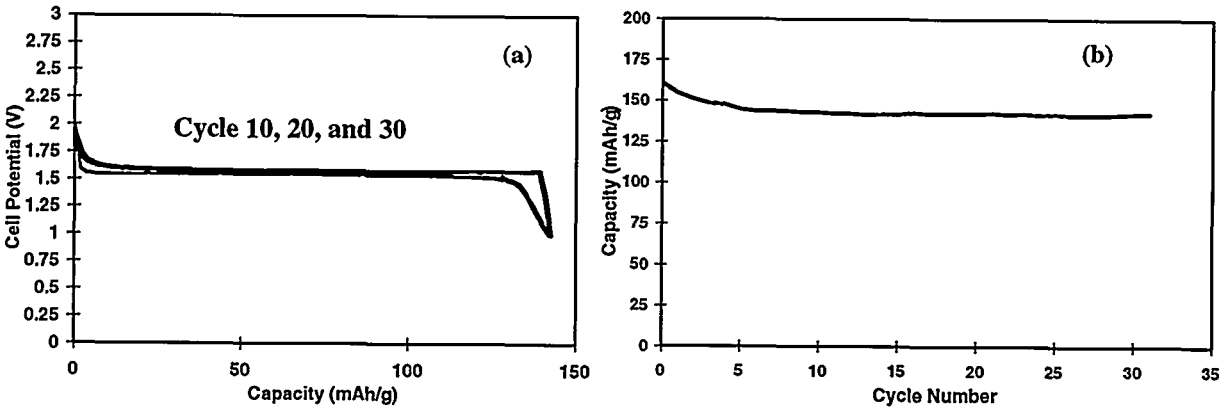

Figure 6

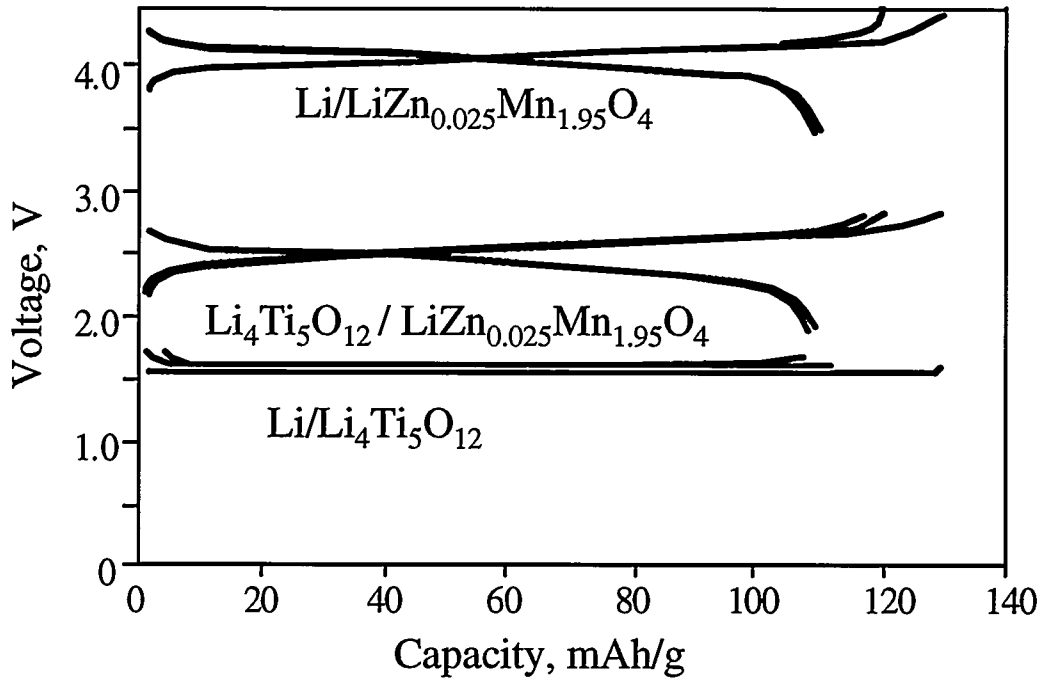

Figure 7

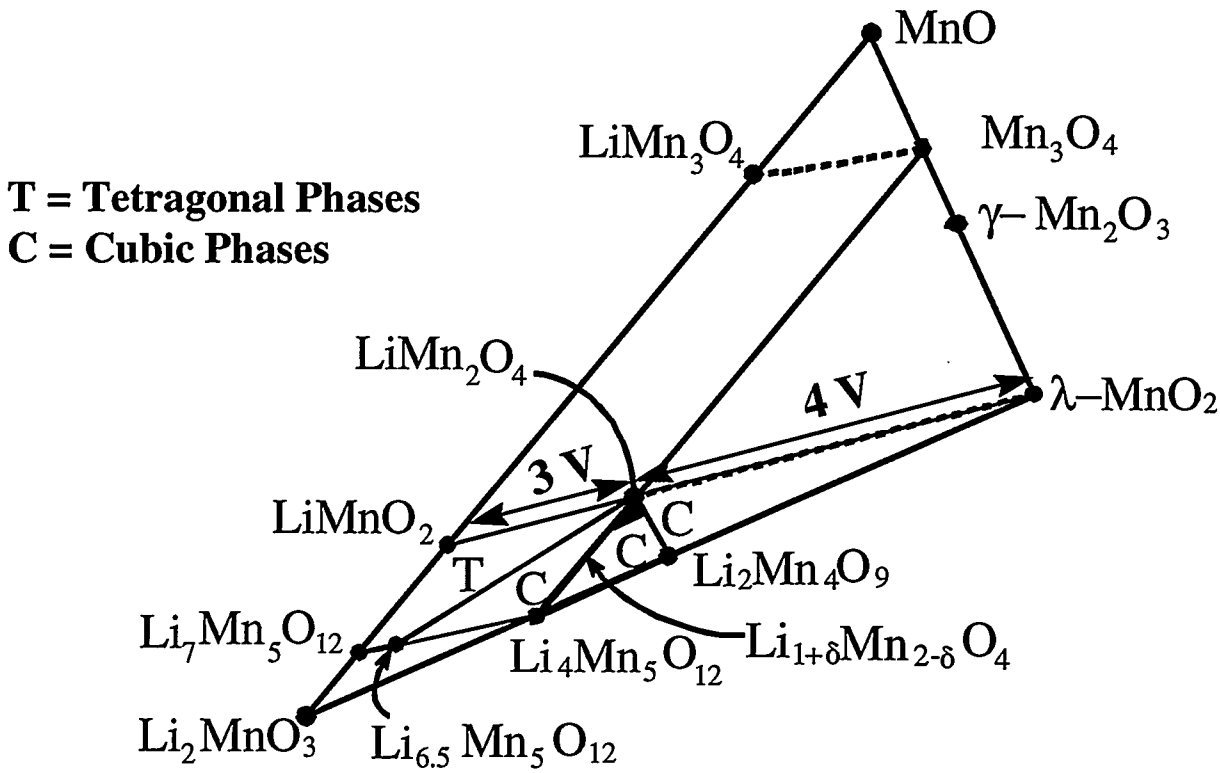

Figure 8

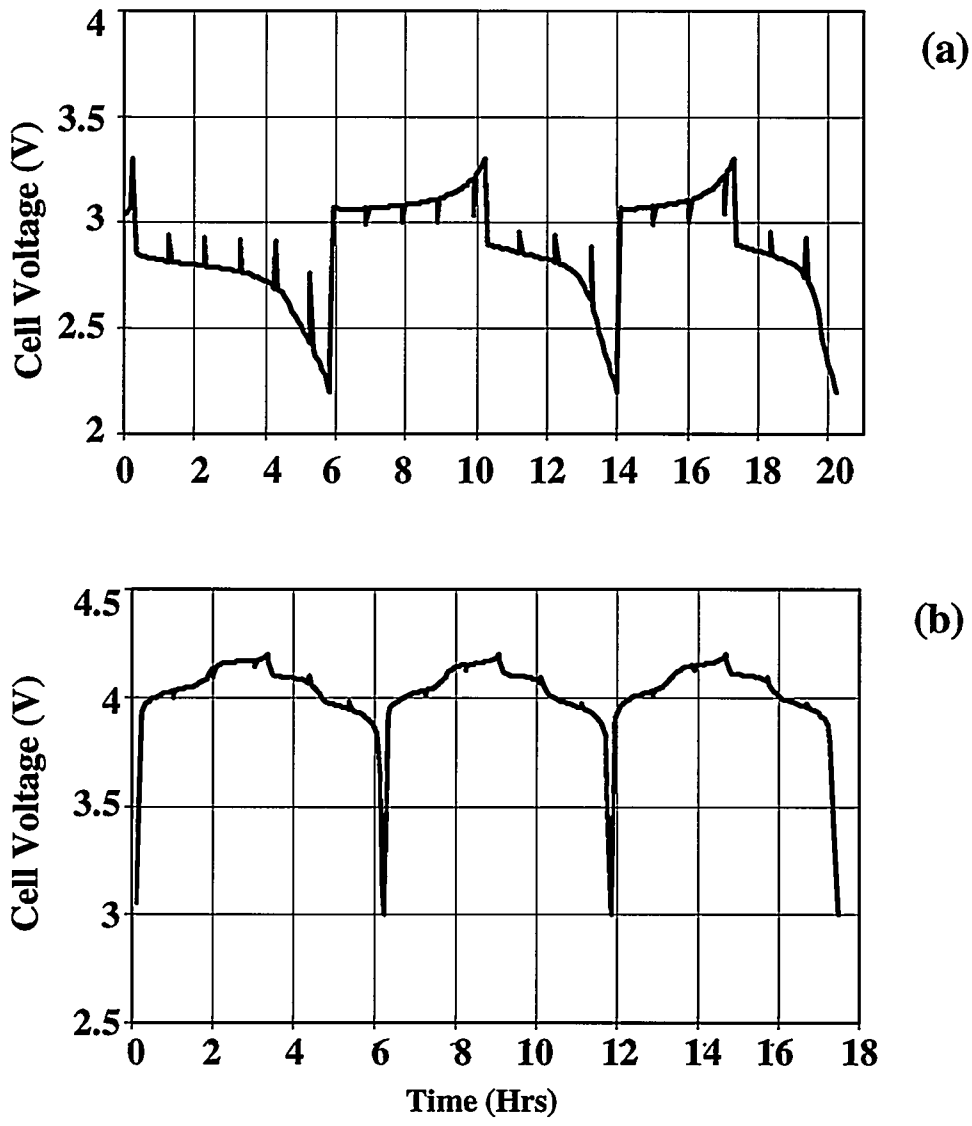
(a)
Cell Voltage (V)
4
3.5
3
2.5
2
0
2
4
6
8
10
12
14
16
18
20
(b)
Cell Voltage (V)
4.5
4
3.5
3
2.5
0
2
4
6
8
10
12
14
16
18
Time (Hrs)

Figure 9

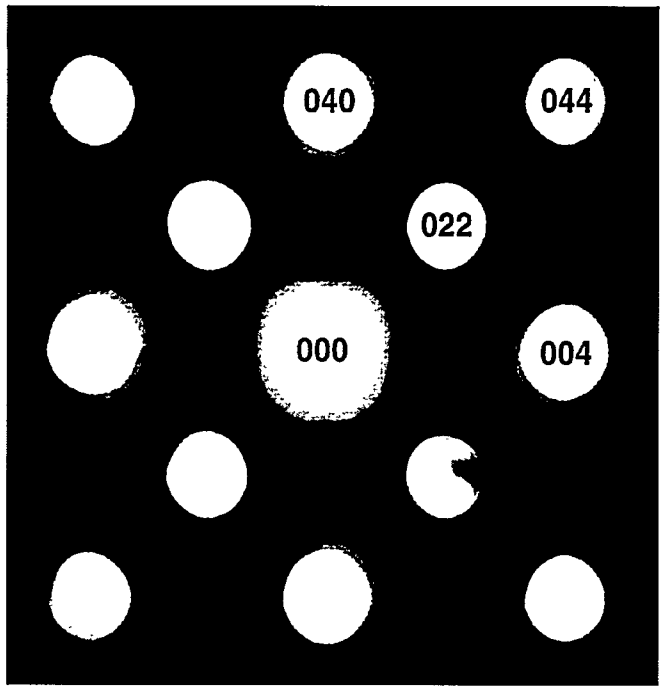

(a)

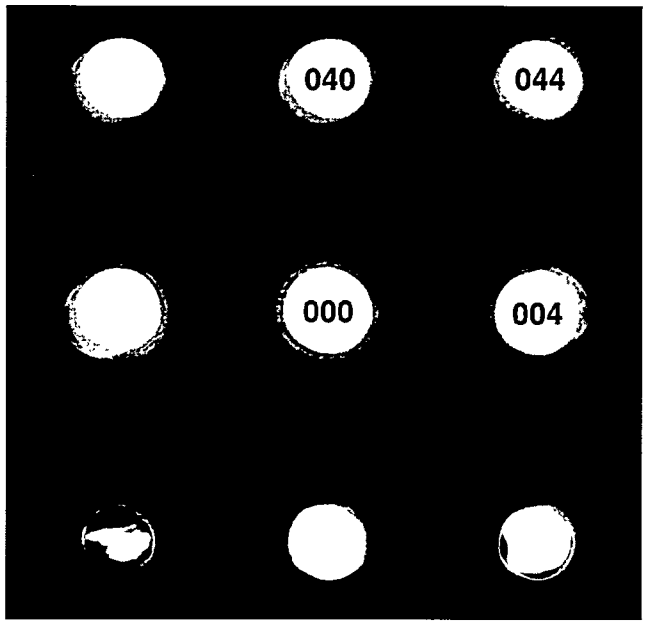

(b)

Figure 10

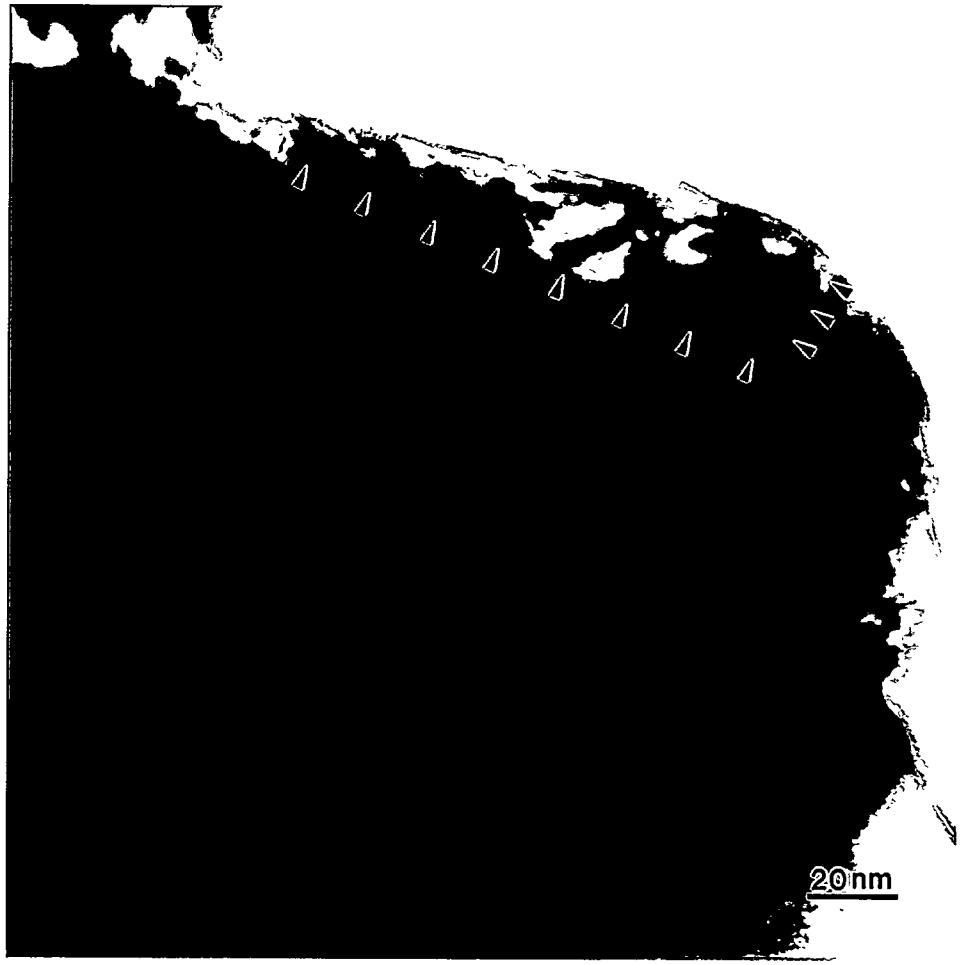

Figure 11

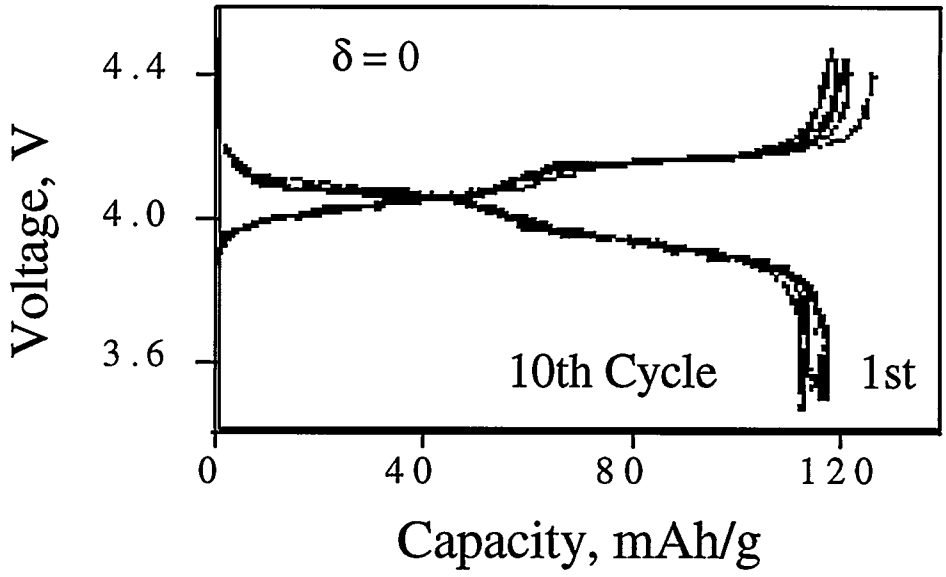
δ = 0
4.4
4.0
3.6
Voltage, V
10th Cycle
1st
0
40
80
120
Capacity, mAh/g

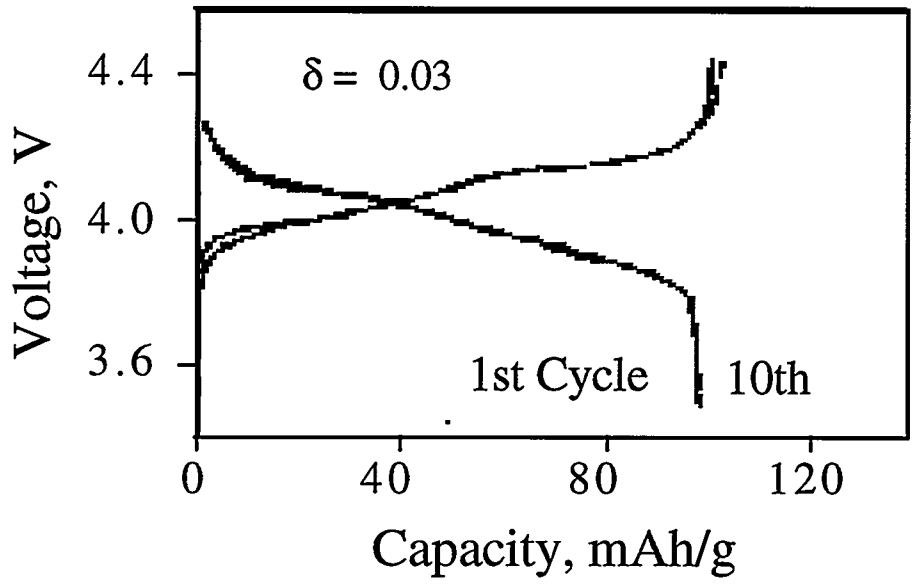
δ = 0.03
4.4
4.0
3.6
Voltage, V
1st Cycle
10th
0
40
80
120
Capacity, mAh/g

Figure 12

(a)

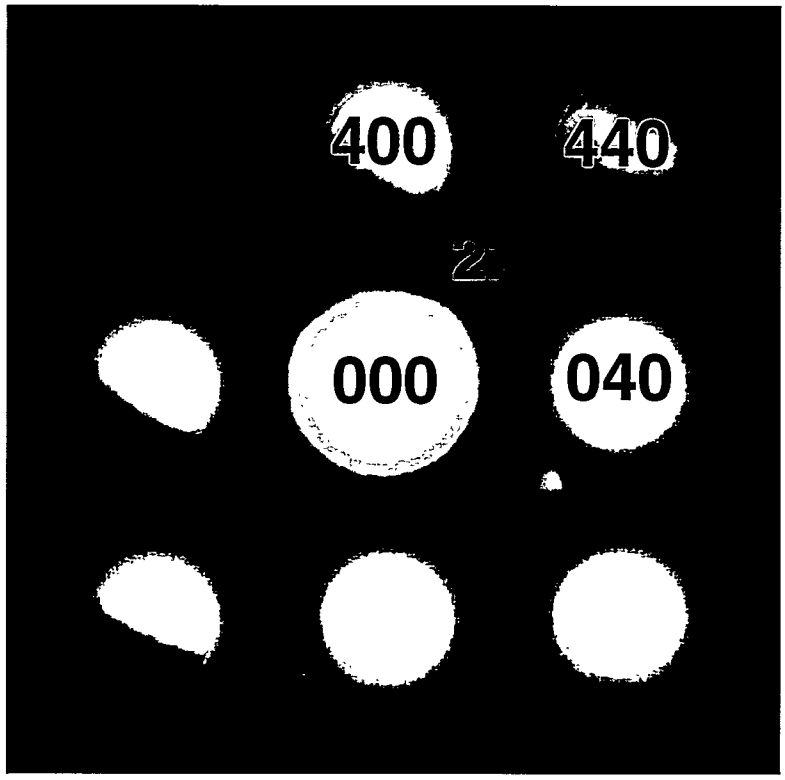

(b)

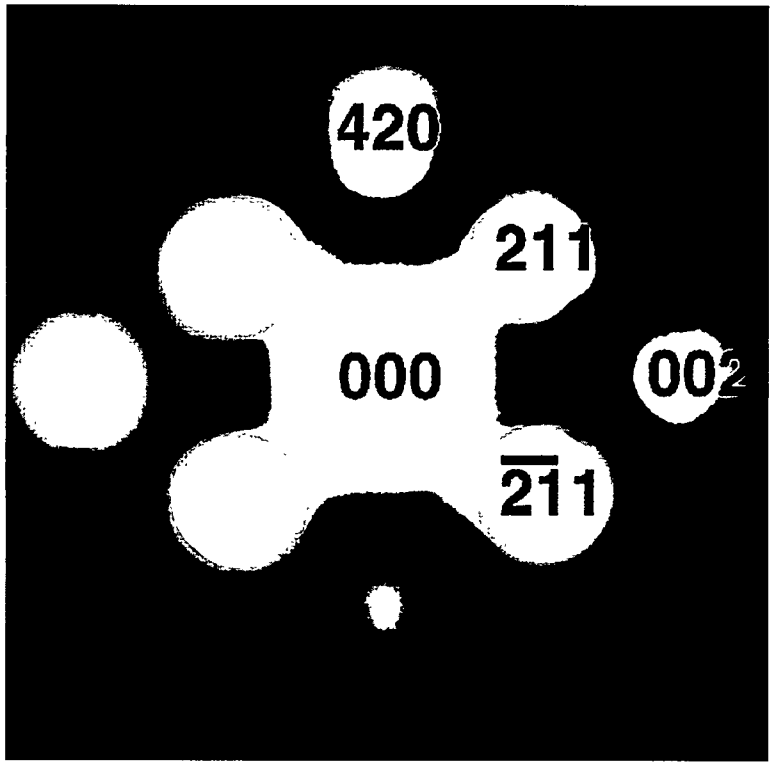

Figure 13

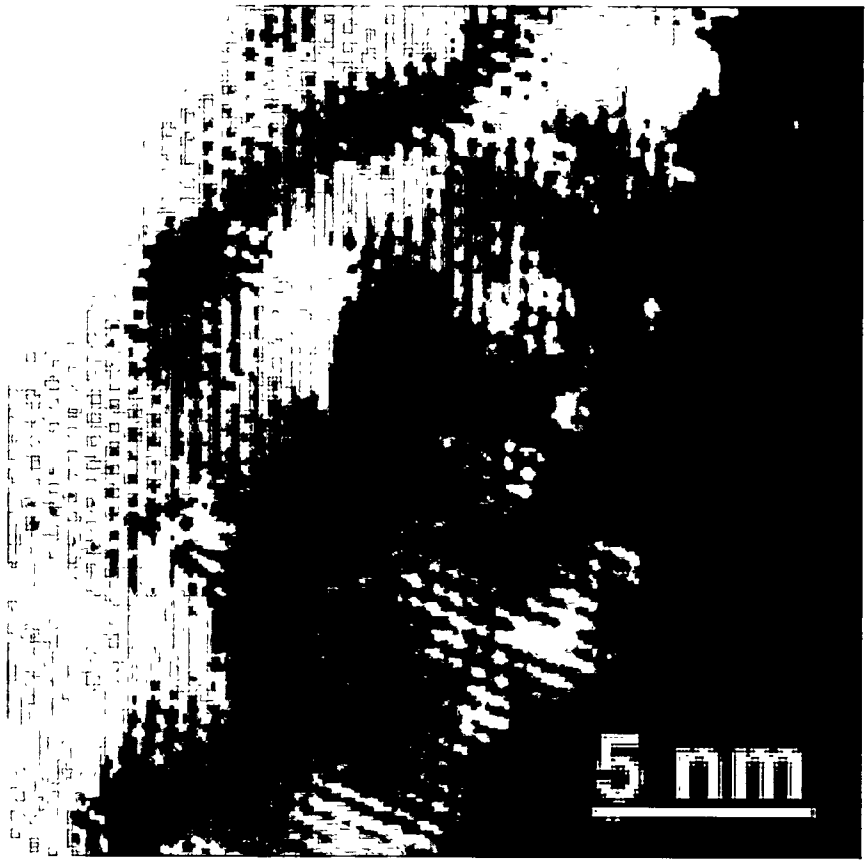

Figure 14